Coupling discrete elements and micropolar continuum through an overlapping region

R.A. Regueiro[1], B. Yan[2]

[1]Department of Civil, Environmental, and Architectural Engineering, University of Colorado at Boulder, 428 UCB, Boulder, CO, 80309; email: regueiro@colorado.edu
[2]Community Surface Dynamics Modeling System, University of Colorado at Boulder, 3100 Marine St., Boulder, CO 80303; email: beichuan.yan@colorado.edu

ABSTRACT

Interfacial mechanics between granular materials and deformable solid bodies involve large shear deformation and grain motion at the interface. To resolve such granular physics at the grain scale in contact with the deformable solid, but in a computationally tractable manner, we present a concurrent multiscale computational method. As a simple problem to verify the method, a one-dimensional string of glued elastic discrete elements is overlapped with a linear elastic micropolar continuum finite element implementation. The overlap coupling is enabled by the bridging scale decomposition method, but now with rotational degrees of freedom (dof) in addition to axial and transverse displacements. The paper presents the preliminaries of coupling discrete element regions and micropolar finite element regions for eventual simulation of granular soil-tire/tool/geosynthetic/penetrometer applications, wherein eventual three-dimensional discrete element formulation and finite strain micromorphic continuum finite element is required.

INTRODUCTION

Granular materials are commonly found in geotechnical applications, and are composites of three phases: solids, liquids, and gases. We limit the modeling currently to single phase (solid grains) and dense granular materials (average coordination number ≈ 5). We are interested primarily in modeling the grain to macro-continuum scale response in the large shear deformation interface region between a granular material and deformable solid body. Such interface can be between a granular soil (e.g., sand, Fig.1(a)) and a tire (Fig.2(a)), tool (e.g., bucket, Fig.2(b)), or cone penetrometer (Fig.1(b)[*]).

Granular materials are challenging to model their mechanical behavior across several orders of magnitude in length-scale. An additional modeling challenge is that they can transition from deforming like a solid to flowing like a fluid and vice versa. Examples of such physical transition are the flow of quartz grains around and at the tip of a driven cone penetrometer penetrating sand, and the shoveling of sand/gravel

[*]http://geosystems.ce.gatech.edu/Faculty/Mayne/Research/devices/cpt.htm

(a) image courtesy of Khalid Alshibli, Louisiana State University. (b) Cone penetrometers (see footnote* on previous page for image reference).

Figure 1. (a) Sand grains at 150×. (b) Cone penetrometers.

by a tractor bucket, for instance. These examples each involve material regions where relative neighbor particle motion is 'large' (flowing like a fluid) and regions where relative neighbor particle motion is 'small' (deforming like a solid).

Using solely "brute force" physics-based simulation methods (such as the discrete element (DE) method [Cundall and Strack, 1979]), it is too computationally intensive to account for the grain-scale mechanical behavior at the macro-scale of these geotechnical engineering applications. Thus, we attempt to restrict the DE region to only where we need it: at the interface of granular material and deformable solid body (i.e., soil-penetrometer, soil-tool, soil-geosynthetic, or soil-tire interface). The computational mechanics modeling challenge is how to couple a DE region to a finite element (FE) region representing the granular material as a continuum further from the interface with the deformable solid, and to do this without introducing artificial boundary effects on the DE region (that in turn contacts the deformable solid shearing through the granular material). We resort to a concurrent multiscale computational modeling approach [Regueiro and Yan, 2010] that retains an "open window" computationally on the grain-scale region adjacent to the deformable solid, while transitioning through an overlap coupling region to a higher order continuum FE method (see Fig.3). The higher order continuum in this paper is limited to a small strain linear isotropic elastic micropolar continuum [Eringen, 1968], whereas a finite strain pressure-sensitive micromorphic elastoplasticity model [Regueiro, 2009] would provide a more suitable higher order continuum framework through which to couple to the DE region. The micropolar continuum is limited to micro-rotations, whereas the micromorphic continuum [Eringen, 1999] introduces also micro-shear and micro-dilation/compaction which are useful for representing the mechanics of *micro-clusters* of grains in a granular material.

A realistic geotechnical engineering application of this multiscale approach is to simulate, with grain-scale resolution, the initial boundary value problem (IBVP) of cone penetrometer penetration (Fig.1(b)). This will allow a physics-based approach to estimating the shear strength of a sandy soil, rather than the traditional empirical approaches. During the penetration, particles can crush, displace and flow to accom-

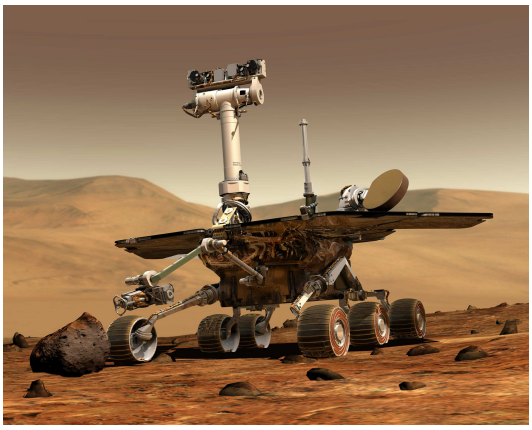

(a) Mars exploration rover: tire interaction with Martian soil (photo source NASA).

(b) loader bucket scooping gravel (`www.dymaxinc.com`).

Figure 2. (a) Soil-tire, and (b) soil-tool interface problems.

modate the cone penetrometer penetrating the sand. This is a complex IBVP, whose interpretation will benefit by a grain-scale computational simulation approach. The multiscale approach will attempt to alleviate the artificial boundary effects [Yan et al., 2010] on an assembly of discrete elements surrounding the cone penetrometer (like in Fig.3). The various soil conditions will come in naturally through constitutive models that handle effects of moisture content, degree of saturation, percentage of clay versus sand, etc. The difference is that the constitutive model is formulated within a micromorphic continuum theory [Regueiro, 2009]. This is a good example of how the multiscale method discussed in this paper can be used to minimize computational effort by maintaining the DE particle region only at the interface with the cone penetrometer, while the micromorphic continuum FE will provide the transition to the continuum region. The micromorphic continuum has more dofs than the standard continuum, but far fewer than the DE region, so it will introduce computational efficiency to the problem.

As a simplified version—for verification purposes—of the concurrent computational multiscale modeling approach presented in Regueiro and Yan [2010], we glue a one-dimensional string of elastic spherical discrete elements, and simplify a micropolar continuum using one-dimensional (1D) Timoshenko beam kinematics with axial stretch [Pinsky, 2001]. The coupling approach then overlaps these two representations of 1D glued grains to test the computational multiscale method.

Bold-face letters denote matrices, tensors and vectors; the symbol "$\cdot$" denotes an inner product of two vectors ($\boldsymbol{a}\cdot\boldsymbol{b}=a_ib_i$), or a single contraction of adjacent indices of two tensors ($\boldsymbol{c}\cdot\boldsymbol{d}=c_{ij}d_{jk}$). Summation is implied on repeated indices. We will assume Cartesian coordinates and small deformations.

1D GLUED DISCRETE ELEMENTS

Consider a one-dimensional string of glued elastic spherical particles (simplification of grains of a granular material). A particle α has axial displacement q_x^α (m) positive in x, transverse displacement q_x^α (m) positive in y, and rotation ω^α (rad) posi-

tive right hand rule about the z (out of page) axis. Consider two particles α and β glued elastically at contact ε, and particles α and γ glued elastically at contact κ. Using Hertz-Mindlin theory for two elastic spheres in contact [Mindlin, 1949], the nonlinear matrix-vector form of balance of linear and angular momentum for particle α is

$$\begin{aligned} &\boldsymbol{m}^{\alpha}\cdot\ddot{\boldsymbol{q}}^{\alpha}+\boldsymbol{f}^{INT,\alpha}(\boldsymbol{q}^{\alpha},\boldsymbol{q}^{\beta},\boldsymbol{q}^{\gamma})=\boldsymbol{f}^{EXT,\alpha} \\ &\boldsymbol{m}^{\alpha}=\begin{bmatrix} m & 0 & 0 \\ 0 & m & 0 \\ 0 & 0 & m_{\omega} \end{bmatrix},\ \ddot{\boldsymbol{q}}^{\alpha}=\begin{bmatrix} \ddot{q}_x^{\alpha} \\ \ddot{q}_y^{\alpha} \\ \ddot{\omega}^{\alpha} \end{bmatrix},\ \boldsymbol{f}^{INT,\alpha}=\begin{bmatrix} f_x^{INT,\alpha}=f_x^{\varepsilon}-f_x^{\kappa} \\ f_y^{INT,\alpha}=f_y^{\varepsilon}-f_y^{\kappa} \\ f_{\omega}^{INT,\alpha}=f_{\omega}^{\varepsilon}-f_{\omega}^{\kappa} \end{bmatrix} \end{aligned} \tag{1}$$

where $\boldsymbol{f}^{EXT,\alpha}$ is the external force. Assembling (1) over all particles, we arrive at the matrix-vector form of balance of linear and angular momentum for the whole 1D glued assembly of spherical particles:

$$\boldsymbol{M}^{Q}\cdot\ddot{\boldsymbol{Q}}+\boldsymbol{F}^{INT,Q}(\boldsymbol{Q})=\boldsymbol{F}^{EXT,Q} \tag{2}$$

where superscript Q implies a discrete element particle variable. These discrete particle equations (2) can be written in energy form to make the partitioning of energy in the overlap region more straightforward for the coupling method described later. For these particle equations, we have

$$\frac{d}{dt}\left(\frac{\partial T^{Q}}{\partial\dot{\boldsymbol{Q}}}\right)-\frac{\partial T^{Q}}{\partial\boldsymbol{Q}}+\frac{\partial U^{Q}}{\partial\boldsymbol{Q}}=\boldsymbol{F}^{EXT,Q} \tag{3}$$

where T^{Q} is the kinetic energy and U^{Q} the potential energy, such that

$$T^{Q}=\frac{1}{2}\dot{\boldsymbol{Q}}\boldsymbol{M}^{Q}\dot{\boldsymbol{Q}}\ ,\ U^{Q}(\boldsymbol{Q})=\int_{\boldsymbol{0}}^{\boldsymbol{Q}}\boldsymbol{F}^{INT,Q}(\boldsymbol{S})d\boldsymbol{S} \tag{4}$$

Carrying out the derivatives in (3), and using the Second Fundamental Theorem of Calculus for $\partial U^{Q}/\partial\boldsymbol{Q}$, leads to (2). Note that no dissipation function appears in (3) because we ignore inter-particle damping for purely elastic particles.

2D LINEAR ELASTIC MICROPOLAR CONTINUUM

The balance equations for a small strain micropolar continuum are the balance of linear and angular momentum, written as [Eringen, 1968]

$$\sigma_{lk,l}+\rho b_k-\rho\dot{v}_k = 0 \tag{5}$$

$$m_{lk,l}+e_{kmn}\sigma_{mn}+\rho\ell_k-\rho\dot{\beta}_k = 0 \tag{6}$$

where

$$m_{lk}n_l da \overset{\text{def}}{=} e_{abk}\int_{da}\sigma'_{lb}\xi_a n'_l da' \tag{7}$$

$$\rho\ell_k dv \overset{\text{def}}{=} e_{abk}\int_{dv}\rho' f'_b\xi_a dv' \tag{8}$$

and σ_{lk} is the unsymmetric Cauchy stress tensor over body $\mathcal{B}$, ρ is the mass density, b_k is a body force per unit mass, v_k is the spatial velocity vector, m_{lk} is the unsymmetric

couple stress, e_{kmn} is the permutation operator [Holzapfel, 2000], ℓ_k is the body couple per unit mass, β_k is the intrinsic spin per unit mass, σ'_{lb} is the symmetric Cauchy stress tensor in micro-element volume dv', ρ' is the micro-element mass density over dv, f'_k is a body force per unit mass in dv', indices $k,l,\cdots = 1,2,3$, and $(\bullet)_{,l} = \partial(\bullet)/\partial x_l$ denotes partial differentiation with respect to the spatial coordinate x_l.

Introducing $w_k = \delta u_k$ and $\eta_k = \delta\varphi_k$ as weighting functions for the macro-displacement vector u_k and micro-rotation vector φ_k, respectively, we apply the Method of Weighted Residuals to formulate the partial differential equations in (5) and (6) into weak form [Hughes, 1987]. The weak, or variational, equations then result, ignoring the body force terms $b_k = 0$ and $\ell_k = 0$, as

$$\int_{\mathcal{B}} \rho w_k \dot{v}_k dv + \int_{\mathcal{B}} w_{k,l}\sigma_{lk} dv = \int_{\Gamma_t} w_k t_k da \tag{9}$$

$$\int_{\mathcal{B}} \rho \eta_k \dot{\beta}_k dv + \int_{\mathcal{B}} \eta_{k,l} m_{lk} dv - \int_{\mathcal{B}} \eta_k \varepsilon_{kmn}\sigma_{mn} dv = \int_{\Gamma_T} \eta_k T_k da \tag{10}$$

where $\mathcal{B}$ is the volume of the continuum body, $t_k = \sigma_{lk}n_l$ is the applied traction on the portion of the boundary Γ_t with outward normal vector n_l, and $T_k = m_{lk}n_l$ is the applied surface couple on the portion of the boundary Γ_T. The linear isotropic elastic micropolar constitutive equations are [Eringen, 1968]

$$\begin{aligned} \sigma_{kl} &= \lambda\varepsilon_{rr}\delta_{kl} + (2\mu+\kappa)\varepsilon_{kl} + \kappa e_{klm}(r_m - \varphi_m) \\ &\quad \varepsilon_{kl} = (u_{k,l} + u_{l,k})/2\,,\; r_m = e_{mab}u_{b,a}/2 \end{aligned} \tag{11}$$

$$m_{kl} = \alpha\varphi_{r,r}\delta_{kl} + \beta\varphi_{k,l} + \gamma\varphi_{l,k} \tag{12}$$

where λ and μ are the Lame parameters, and κ, α, β, and γ are additional elastic parameters. The next section simplifies this linear elastic micropolar continuum for 1D Timoshenko beam kinematics with axial stretch.

1D TIMOSHENKO BEAM KINEMATICS FOR 2D MICROPOLAR CONTINUUM

Adapting the Timoshenko beam kinematics from Pinsky [2001] by adding an axial stretch dof u, the small strain displacement vector $\boldsymbol{u}$ and micro-rotation vector $\boldsymbol{\varphi}$ are

$$\boldsymbol{u} = \begin{bmatrix} u_1 \\ u_2 \\ u_3 \end{bmatrix} = \begin{bmatrix} u(x_1) - x_2\theta(x_1) \\ v(x_1) \\ 0 \end{bmatrix},\; \boldsymbol{\varphi} = \begin{bmatrix} 0 \\ 0 \\ \theta(x_1) \end{bmatrix} \tag{13}$$

The small strain tensor then becomes

$$\boldsymbol{\epsilon} = \begin{bmatrix} u_{,1} - x_2\theta_{,1} & \gamma^{sh}/2 & 0 \\ \gamma^{sh}/2 & 0 & 0 \\ 0 & 0 & 0 \end{bmatrix} \tag{14}$$

where $(\bullet)_{,1} = \partial(\bullet)/\partial x_1 = \partial(\bullet)/\partial x = (\bullet)_{,x}$, and shearing $\gamma^{sh} = v_{,1} - \theta$. It can then be shown from (11,12) that the nonzero stress components are

$$\sigma_{11} = (\lambda + 2\mu + \kappa)\varepsilon_{11} \; , \; \sigma_{12} = (\mu + \kappa)\gamma^{sh} \; , \; \sigma_{21} = \mu\gamma^{sh} \; , \; m_{13} = \gamma\theta_{,1} \; , \; m_{31} = \beta\theta_{,1} \quad (15)$$

where $\sigma_{22} = \sigma_{33} = \sigma_{23} = \sigma_{32} = \sigma_{13} = \sigma_{31} = 0$ and $m_{11} = m_{22} = m_{33} = m_{12} = m_{21} = m_{23} = m_{32} = 0$. The couple stress m_{13} is a moment acting on the x_1 face in the x_3 direction. The m_{31} stress does not appear in the final form of the balance equations. The balance equations simplify to

$$\sigma_{11,1} - \rho\ddot{u}_1 = 0 \quad (16)$$

$$\sigma_{12,1} - \rho\ddot{u}_2 = 0 \quad (17)$$

$$m_{13,1} + \sigma_{12} - \sigma_{21} - \rho\dot{\beta}_3 = 0 \quad (18)$$

There are three equations and three unknowns: u, v, and θ. We substitute into the coupled weak form (9,10), express in Galerkin form [Hughes, 1987], and interpolate the displacements and rotations as

$$u^h(x,t) = \boldsymbol{N}^{e,u}(x) \cdot \boldsymbol{d}^e_x(t) \; , \; v^h(x,t) = \boldsymbol{N}^{e,v}(x) \cdot \boldsymbol{d}^e_y(t) \; , \; \theta^h(x,t) = \boldsymbol{N}^{e,\theta}(x) \cdot \boldsymbol{d}^e_\theta(t) \quad (19)$$

where we use a mixed formulation for shape function matrices $\boldsymbol{N}^{e,u}$, $\boldsymbol{N}^{e,v}$, and $\boldsymbol{N}^{e,\theta}$, and e implies element variable. The coupled finite element matrix form, after element assembly and application of BCs, results as

$$\boldsymbol{M}^D \cdot \ddot{\boldsymbol{D}} + \boldsymbol{F}^{INT,D}(\boldsymbol{D}) = \boldsymbol{F}^{EXT,D} \quad (20)$$

$$\boldsymbol{M}^D = \begin{bmatrix} \boldsymbol{M}^{uu} & \boldsymbol{0} & -\boldsymbol{M}^{u\theta} \\ \boldsymbol{0} & \boldsymbol{M}^{vv} & \boldsymbol{0} \\ -\boldsymbol{M}^{\theta u} & \boldsymbol{0} & \boldsymbol{M}^{\theta\theta} \end{bmatrix} \quad \boldsymbol{D} = \begin{bmatrix} \boldsymbol{d}_u \\ \boldsymbol{d}_v \\ \boldsymbol{d}_\theta \end{bmatrix} \; , \boldsymbol{F}^{INT,D} = \boldsymbol{K}^D \cdot \boldsymbol{D}$$

$$\boldsymbol{K}^D = \begin{bmatrix} \boldsymbol{K}^{uu} & \boldsymbol{0} & -\boldsymbol{K}^{u\theta} \\ \boldsymbol{0} & \boldsymbol{K}^{vv} & -\boldsymbol{K}^{v\theta} \\ -\boldsymbol{K}^{\theta u} & -\boldsymbol{K}^{\theta v} & \boldsymbol{K}^{\theta\theta} \end{bmatrix} \quad \boldsymbol{F}^{EXT,D} = \begin{bmatrix} \boldsymbol{F}_F \\ \boldsymbol{F}_V \\ \boldsymbol{F}_M + \boldsymbol{F}_{M^\theta} \end{bmatrix}$$

where $\boldsymbol{M}^D$ is symmetric, but $\boldsymbol{K}^D$ is unsymmetric. The submatrices of $\boldsymbol{M}^D$ and $\boldsymbol{K}^D$ couple u, v, and θ. These discrete FE equations (20) can be written in energy form to make the partitioning of energy in the overlap region for coupling more straightforward. For these FE equations, we have

$$\frac{d}{dt}\left(\frac{\partial T^D}{\partial \dot{\boldsymbol{D}}}\right) - \frac{\partial T^D}{\partial \boldsymbol{D}} + \frac{\partial U^D}{\partial \boldsymbol{D}} = \boldsymbol{F}^{EXT,D} \quad (21)$$

where T^D is the kinetic energy and U^D the potential energy, such that

$$T^D = \frac{1}{2}\dot{\boldsymbol{D}}\boldsymbol{M}^D\dot{\boldsymbol{D}} \, , U^D(\boldsymbol{D}) = \int_{\boldsymbol{0}}^{\boldsymbol{D}} \boldsymbol{F}^{INT,D}(\boldsymbol{S}) d\boldsymbol{S} \quad (22)$$

Carrying out the derivatives in (21), and using the Second Fundamental Theorem of Calculus for $\partial U^D/\partial \boldsymbol{D}$, leads to (20). The next section presents the coupling methodology for kinematics and energy.

COUPLING

Following some of the same notation presented in Klein and Zimmerman [2006], we define a generalized dof vector $\breve{\boldsymbol{Q}}$ for particle displacements and rotations in the system as

$$\breve{\boldsymbol{Q}} = [\boldsymbol{q}_\alpha, \boldsymbol{q}_\beta, \ldots, \boldsymbol{q}_\gamma, \omega_\alpha, \omega_\beta, \ldots, \omega_\gamma]^T, \ \alpha, \beta, \ldots, \gamma \in \breve{\mathcal{A}} \tag{23}$$

where $\boldsymbol{q}_\alpha$ is the displacement vector of particle α, ω_α its rotation, and $\breve{\mathcal{A}}$ is the set of all particles. Likewise, the finite element nodal displacements and rotations are written as

$$\breve{\boldsymbol{D}} = [\boldsymbol{d}_a, \boldsymbol{d}_b, \ldots, \boldsymbol{d}_c, d_{\theta,a}, d_{\theta,b}, \ldots, d_{\theta,c}]^T, \ a, b, \ldots, c \in \breve{\mathcal{N}} \tag{24}$$

where $\boldsymbol{d}_a$ is the displacement vector of node a, $d_{\theta,a}$ is the rotation of node a, $\breve{\mathcal{N}}$ is the set of all nodes. In order to satisfy the boundary conditions for both regions, the motion of the particles in the overlap region (referred to as "ghost particles," red particles in Fig.3) is prescribed by the continuum displacement and rotation fields. Referring to Fig.3, the prescribed particle motions $\widehat{\boldsymbol{Q}}$ can be viewed as constraints on the free particle region, and likewise the prescribed finite element nodal displacements and rotations $\widehat{\boldsymbol{D}}$ can be viewed as constraints on the finite element mesh in the overlap region.

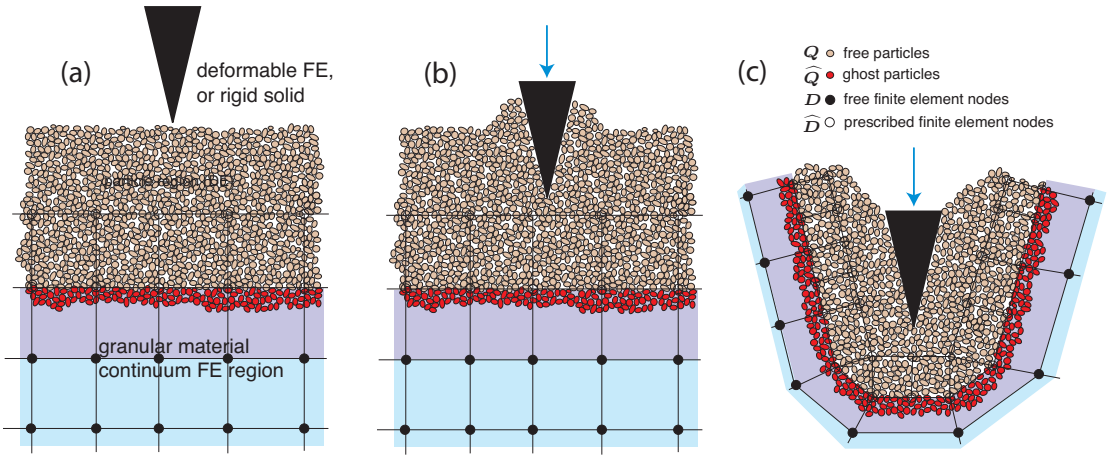

Figure 3. Illustration of adaptivity and coupling. In (a), a deformable or rigid solid body approaches the granular material, and in (b) it begins to shear/penetrate the granular material in the DE particle region. In (c), the solid body has sheared the particle region enough that the FE mesh is re-meshed adaptively and the particle region is extended. Adaptivity [Nie et al., 2010] is a means to change the nodal coordinates of a mesh if the mesh is highly distorted, in this case to keep the DE particle region at the interface of the deformable solid while allowing the elements not to distort too much.

In general, the displacement vector of a particle α can be represented by the finite element interpolation of the continuum displacement field $\boldsymbol{u}^h$ evaluated at the particle centroid x_α, such that

$$\boldsymbol{u}^h(x_\alpha, t) = \sum_{a \in \breve{\mathcal{N}}} N_a^u(x_\alpha)\boldsymbol{d}_a(t) \quad \alpha \in \breve{\mathcal{A}} \tag{25}$$

where N_a^u are the shape functions associated with the continuum displacement field $\boldsymbol{u}^h$. Recall that N_a^u have compact support and thus are only evaluated for particles with centroids that lie within an element containing node a in its domain. In DE, particle dofs (translations and rotations) are tracked at the particle centroids. For example, we can write the prescribed displacement of ghost particle α as

$$\boldsymbol{q}_\alpha(t) = \boldsymbol{u}^h(x_\alpha, t) = \sum_{a \in \check{\mathcal{N}}} N_a^u(x_\alpha)\boldsymbol{d}_a(t) \quad \alpha \in \widehat{\mathcal{A}} \tag{26}$$

Likewise, particle rotation vectors can be represented by the finite element interpolation of the continuum micro-rotation field θ^h evaluated at the particle centroid x_α. For all ghost particles (Fig.3), the interpolations can be written as

$$\widehat{\boldsymbol{Q}} = \boldsymbol{N}_{\widehat{Q}D} \cdot \boldsymbol{D} + \boldsymbol{N}_{\widehat{Q}\widehat{D}} \cdot \widehat{\boldsymbol{D}} \tag{27}$$

where $\boldsymbol{N}_{\widehat{Q}D}$ and $\boldsymbol{N}_{\widehat{Q}\widehat{D}}$ are shape function matrices containing individual nodal shape functions N_a^u and N_b^θ. We assume the total kinetic and potential energy of the coupled particle-continuum system may be written as the sum of the energies

$$T(\dot{\boldsymbol{Q}}, \dot{\boldsymbol{D}}) = T^Q(\dot{\boldsymbol{Q}}, \dot{\widehat{\boldsymbol{Q}}}(\dot{\boldsymbol{Q}}, \dot{\boldsymbol{D}})) + T^D(\dot{\boldsymbol{D}}, \dot{\widehat{\boldsymbol{D}}}(\dot{\boldsymbol{Q}})) \tag{28}$$

$$U(\boldsymbol{Q}, \boldsymbol{D}) = U^Q(\boldsymbol{Q}, \widehat{\boldsymbol{Q}}(\boldsymbol{Q}, \boldsymbol{D})) + U^D(\boldsymbol{D}, \widehat{\boldsymbol{D}}(\boldsymbol{Q})) \tag{29}$$

where we have indicated the functional dependence of the prescribed particle motion and nodal dofs solely upon the free particle motion and nodal dofs $\boldsymbol{Q}$ and $\boldsymbol{D}$, respectively.

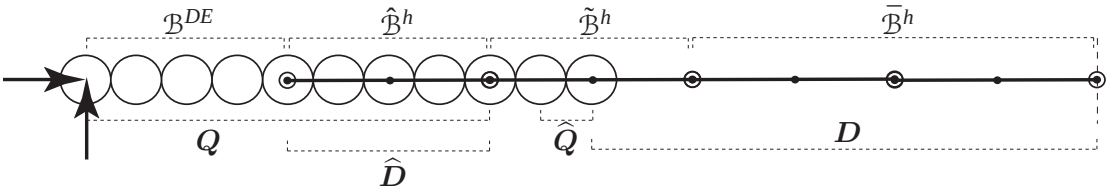

Figure 4. 1D string of 11 elastic spheres overlapped partially by 4 1D micropolar continuum FEs. Free particle dofs are indicated by $\boldsymbol{Q}$, ghost particle dofs by $\widehat{\boldsymbol{Q}}$, prescribed FE nodal dofs by $\widehat{\boldsymbol{D}}$, and free FE nodal dofs by $\boldsymbol{D}$. $\mathcal{B}^{DE}$ is the pure particle domain (no overlapping FE mesh), $\hat{\mathcal{B}}^h$ the overlapping FE domain where nodal dofs are completely prescribed, $\tilde{\mathcal{B}}^h$ the overlapping FE domain where particle motions and nodal dofs are prescribed and free nodal dofs exist, and $\bar{\mathcal{B}}^h$ the pure continuum FE domain with no underlying particles.

NUMERICAL EXAMPLES

The one-dimensional overlapped coupled domain in Fig.4 is compressed axially and sheared in the transverse direction as indicated in the figure. The particles are assumed to be isotropic elastic quartz (E =2.9e10 Pa, ν =0.25), and likewise for corresponding parameters of the 1D micropolar continuum (the additional micropolar elastic parameters are scaled to these parameters). Preliminary results of the coupling response is shown in Fig.5. It can be seen that if the elastic stiffnesses of the 1D micropolar continuum rod finite element mesh are not scaled, the response is too stiff,

and the partitioning of energy via a volume fraction in the overlapped region $\tilde{\mathcal{B}}^h$ will not lead to a smooth displacement field along the rod. When scaled, the homogeneous axial displacement along the bar can be achieved, however, the transverse displacement still demonstrates an artificial boundary effect for the transverse displacement and force when the stiffnesses are scaled. These are preliminary results, and we are in the process of rectifying the scaling for the transverse dof.

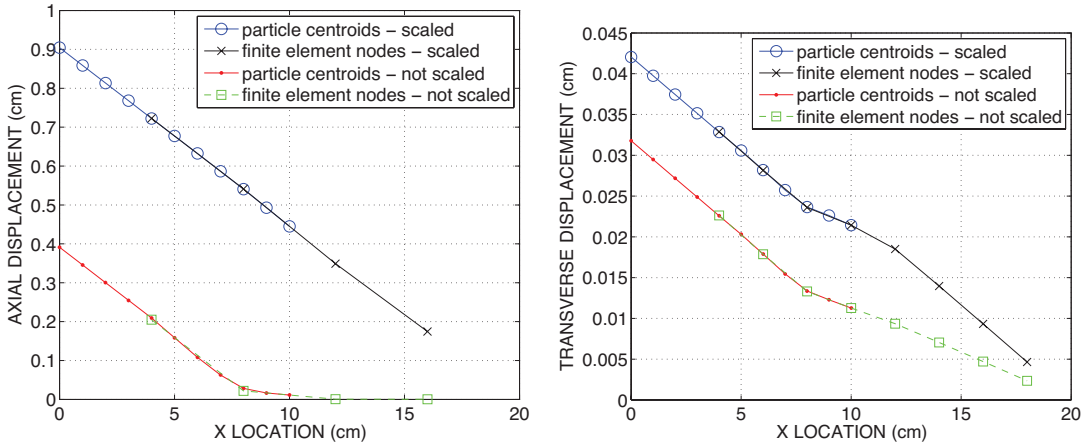

Figure 5. (left) Axial displacement versus position along the 1D string of particles and FE mesh. (right) Transverse displacement.

CONCLUSION

This short paper focussed on the formulation of the discrete particle and micropolar FE balance equations simplified for linear elasticity and 1D Timoshenko beam kinematics, and coupling methodology for concurrent multiscale computational approach for physics-based modeling of interfacial mechanics between deformable solids and granular materials (dry and dense). Numerical examples showed preliminary results of the coupling method for addressing artificial boundary effects at the transition between DE and FE regions.

Ultimately, a fundamental understanding of granular physics interacting with a solid body can lead to improved design of devices for granular soil-machine tool, soil-tire, soil-geosynthetic, and soil-penetrometer interaction. The practicing geotechnical engineer should be aware that such advanced modeling methods could reduce uncertainty in the future when interpreting cone penetrometer results for estimating shear strength in sand, or designing a new geosynthetic to reinforce a granular soil. There is still a need to validate this multiscale modeling approach against experiment data that bridges the grain-scale to the 'small' continuum scale, which is ongoing work as part of a research collaboration with Professor Khalid Alshibli at Louisiana State University through the NSF grant indicated in the Acknowledgements.

ACKNOWLEDGEMENTS

Funding for this research was provided by National Science Foundation grant CMMI-0700648, Army Research Office grant W911NF-09-1-0111, and the Army Research Laboratory. This funding is gratefully acknowledged.

REFERENCES

P. Cundall and O.D.L. Strack. A discrete numerical model for granular assemblies. *Geotechnique*, 29:47–65, 1979.

A.C. Eringen. Theory of Micropolar Elasticity. In H. Liebowitz, editor, *Fracture, An Advanced Treatise*, volume 2, pages 622–729. Academic Press, 1968.

A.C. Eringen. *Microcontinuum Field Theories I: Foundations and Solids*. Springer-Verlag, 1999.

G. A. Holzapfel. *Nonlinear Solid Mechanics: A Continuum Approach for Engineering*. John Wiley & Sons, 2000.

T. J. R. Hughes. *The Finite Element Method*. Prentice-Hall: New Jersey, 1987.

P.A. Klein and J.A. Zimmerman. Coupled atomistic-continuum simulations using arbitrary overlapping domains. *J. Comput. Phys.*, 213(1):86 – 116, 2006.

R.D. Mindlin. Compliance of elastic bodies in contact. *J. App. Mech.*, 16(3):259–268, 1949.

J.H. Nie, D.A. Hopkins, Y.T. Chen, and H.T. Hsieh. Development of an object-oriented finite element program with adaptive mesh refinement for multi-physics applications. *Advances in Engineering Software*, 41(4):569 – 579, 2010.

P.M. Pinsky. Finite Element Structural Analysis. unpublished course notes, Stanford University, 2001.

R.A. Regueiro. Finite strain micromorphic pressure-sensitive plasticity. *J. Eng. Mech.*, 135:178–191, 2009.

R.A. Regueiro and B. Yan. Concurrent multiscale computational modeling for dense dry granular materials interfacing deformable solid bodies. In *Springer Series in Geomechanics and Geoengineering*, page in press, 2010.

B. Yan, R.A. Regueiro, and S. Sture. Three dimensional discrete element modeling of granular materials and its coupling with finite element facets. *Eng. Comput.*, 27(4): 519–550, 2010.